Eemian Greenland ice sheet simulated with a higher-order model shows strong sensitivity to SMB forcing

Andreas Plach[1], Kerim H. Nisancioglu[1,2], Petra M. Langebroek[3], Andreas Born[1], and Sébastien Le clec'h[4,5]

[1]Department of Earth Science, University of Bergen and Bjerknes Centre for Climate Research, Bergen, Norway
[2]Centre for Earth Evolution and Dynamics, University of Oslo, Oslo, Norway
[3]NORCE Norwegian Research Centre, Bjerknes Centre for Climate Research, Bergen, Norway
[4]Laboratoire des Sciences du Climat et de l'Environnement, LSCE/IPSL, CEA-CNRS-UVSQ, Université Paris-Saclay, F-91191 Gif-sur-Yvette, France
[5]Earth System Science and Department Geografie, Vrije Universiteit Brussel, Brussels, Belgium

Correspondence to: Andreas Plach (andreas.plach@uib.no)

Abstract. The Greenland ice sheet contributes increasingly to global sea level rise. Its history during past warm intervals is a valuable reference for future sea level projections. We present ice sheet simulations for the Eemian interglacial period (~130,000 to 115,000 years ago), a period with warmer-than-present summer climate over Greenland. The evolution of the Eemian Greenland ice sheet is simulated with a 3D higher-order ice sheet model, forced with a surface mass balance derived from regional climate simulations. Sensitivity experiments with various surface mass balances, basal friction, and ice flow approximations are discussed. The surface mass balance forcing is identified as the controlling factor setting the minimum in Eemian ice volume, emphasizing the importance of a reliable surface mass balance model. Furthermore, the results indicate that the surface mass balance forcing is more important than the representation of ice flow for simulating the large-scale ice sheet evolution. This implies that modeling of the future contribution of the Greenland ice sheet to sea level rise highly depends on an accurate surface mass balance.

1 Introduction

The simulation of the Greenland ice sheet (GrIS) under past warmer climates is a valuable way to test methods used for sea level rise projections. This study investigates ice sheet simulations for the Eemian interglacial period. The Eemian (~130,000 to 115,000 years ago; hereafter 130 to 115 ka) is the most recent warmer-than-present period in Earth's history and thereby provides an analogue for future warmer climates (e.g., Clark and Huybers, 2009; Yin and Berger, 2015). The Eemian summer temperature is estimated to have been 4-5 °C above present over most Arctic land areas (e.g., Capron et al., 2017) and an ice core record from NEEM (the North Greenland Eemian Ice Drilling project in northwest Greenland, NEEM community members, 2013) indicates a local warming of 8.5±2.5 °C (Landais et al., 2016) compared to pre-industrial levels. In spite of this strong warming, total gas content measurements from the Greenland ice cores at GISP2, GRIP, NGRIP, and NEEM indicate an Eemian surface elevation no more than a few hundred meters lower than present (at these locations). NEEM data indicates that the ice thickness in northwest Greenland decreased by 400±250 m between 128 and 122 ka with a surface elevation of 130±300 m

lower than the present at 122 ka, resulting in a modest sea level rise estimate of 2 m (NEEM community members, 2013). Nevertheless, coral reef-derived global mean sea level estimates show values of at least 4 m above the present level (Overpeck et al., 2006; Kopp et al., 2013; Dutton et al., 2015). While this could indicate a reduced Antarctic ice sheet, the contribution from the GrIS to the Eemian sea level highstand remains unclear. Previous modeling studies focusing on Greenland (e.g.,

5 Letréguilly et al., 1991; Otto-Bliesner et al., 2006; Robinson et al., 2011; Born and Nisancioglu, 2012; Stone et al., 2013; Helsen et al., 2013) used very different setup and forcing, and show highly variable results.

Ice sheets lose mass either due to a reduced surface mass balance (SMB) or accelerated ice dynamical processes. Ice dynamical processes may have contributed to the Eemian ice loss, for example through changes in basal conditions, similar to what is seen today and what is discussed for the future of the ice sheet. Zwally et al. (2002) associate surface melt with an acceleration

10 of GrIS flow and argue that surface melt-induced enhanced basal sliding provides a mechanism for rapid, large-scale, dynamic responses of ice sheets to climate warming. Several other studies have attributed the recent and future projected sea level rise from Greenland partly to dynamical responses. Price et al. (2011), for example, use a 3D higher-order model to simulate sea level rise caused by the dynamical response of the GrIS, and they find an upper bound of 45 mm by 2100 (without assuming any changes to basal sliding in the future). This dynamical contribution is of similar magnitude as previously published

15 SMB-induced sea level rise estimates by 2100 (40-50 mm; Fettweis et al., 2008). Pfeffer et al. (2008) provide a sea level rise estimate of 165 mm from the GrIS by 2100 based on a kinematic scenario with doubling ice transport through topographically-constrained outlet glaciers. Furthermore, Robel and Tziperman (2016) present synthetic ice sheet simulations and argue that the early part of the deglaciation of large ice sheets is strongly influenced by an acceleration of ice streams as a response to changes in climate forcing.

20 In this study, we apply a computationally efficient 3D higher-order ice flow approximation (alias Blatter-Pattyn; BP; Blatter, 1995; Pattyn, 2003) implemented in the Ice Sheet System Model (ISSM; Larour et al., 2012; Cuzzone et al., 2018). Including higher-order stress gradients provides a comprehensive ice flow representation to test the importance of ice dynamics for modeling the Eemian GrIS. Furthermore, we avoid shortcomings in regions where simpler ice flow approximations, often used in paleo applications, are inappropriate, especially fast flowing ice in the case of the Shallow Ice Approximation (SIA; Hutter,

25 1983; Greve and Blatter, 2009) and regions dominated by ice creep in the case of the Shallow Shelf Approximation (SSA; MacAyeal, 1989; Greve and Blatter, 2009). The higher-order approximation is equally well suited to simulate slow as well as fast flowing ice.

Plach et al. (2018) show that the derivation of the Eemian SMB strongly depends on the SMB model choice. Here, we test SMB forcing derived from dynamically downscaled Eemian climate simulations and two SMB models (a full surface energy

30 balance model and an intermediate complexity SMB model) as described in Plach et al. (2018). Furthermore, we perform sensitivity experiments varying basal friction for the entire GrIS, and localized changes below the outlet glaciers.

The aim of this study is to compare the impact of SMB and basal sliding on the evolution of the Eemian GrIS. Furthermore, employing a 3D higher-order ice flow model, instead of simpler ice dynamical approximations often used in millennial-scale ice sheet simulations, is a novelty of this study. It allows us to evaluate the importance of the ice flow approximation used for

35 Eemian studies.

2 Models and experimental setup

2.1 SMB methods

The SMB forcing is based on Eemian time slice simulations with a fast version of the Norwegian Earth System Model (NorESM1-F; Guo et al., 2019) representing the climate of 130, 125, 120, and 115 ka using respective greenhouse gas concen-
5 trations and orbital parameters (details in Plach et al., 2018). In the climate model simulations the present-day GrIS topography is used. These global simulations are dynamically downscaled over Greenland with the regional climate model Modèle Atmosphérique Régional (MAR; Gallée and Schayes, 1994; de Ridder and Gallée, 1998; Gallée et al., 2001; Fettweis et al., 2006). Subsequently, the SMB is calculated with (1) a full surface energy balance (SEB) model as implemented within MAR (MAR-SEB) and (2) an intermediate complexity SMB model (MAR-BESSI; BErgen Snow SImulator; BESSI; Born et al., 2019).
10 Both models are physically based SMB models including a snowpack explicitly solving for the impact of solar shortwave radiation (this is essential for the Eemian period which has a significantly different solar insolation compared to today, e.g., van de Berg et al., 2011; Robinson and Goelzer, 2014). MAR-SEB is bidirectionally coupled to the atmosphere of MAR (i.e., evolving SEB impacts atmospheric processes, for example: albedo changes impact surface temperature, cloud cover, and humidity), while MAR-BESSI is uncoupled. These two models are selected as the most plausible Eemian SMBs from a wider
15 range of simulations discussed in Plach et al. (2018); they show a negative total SMB during the Eemian peak warming. While MAR-SEB is chosen as the control because it has been extensively validated against observations in previous studies (Fettweis, 2007; Fettweis et al., 2013, 2017), MAR-BESSI is used to test the sensitivity of the ice sheet simulations to the SMB forcing. MAR-SEB and MAR-BESSI employ a different temporal model time step, while MAR-SEB uses steps of 180 seconds, MAR-BESSI calculates in daily time steps. The longer time steps used by MAR-BESSI imply that extreme temperatures (e.g., lowest
20 temperatures at night can lead to more refreezing) are damped and this is likely the cause for a lower amount of refreezing in MAR-BESSI compared to MAR-SEB. Furthermore, MAR-BESSI uses a simpler albedo representation than MAR-SEB. Lower refreezing and simpler steps in albedo changing from fresh snow to glacier ice are identified as the main reasons for more negative SMB as calculated by MAR-BESSI. For a detailed discussion of the differences between the models the reader is referred to Plach et al. (2018). The two different SMB models are employed to test the sensitivity of the ice sheet simulations
25 to the prescribed SMB forcing.

All SMB time slice simulations are calculated offline using the modern ice surface elevation, given the lack of data constraining the configuration of the Eemian GrIS surface elevation. The evolution of the SMB with the changing ice surface elevation is simulated with local SMB-altitude gradients following Helsen et al. (2012, 2013). The SMB gradient method is used to calculate SMB-altitude gradients at each grid point from the surrounding grid points within a default radius of 150 km
30 (linear regression of SMB vs. altitude). Since the SMB-altitude gradients in the accumulation and the ablation zones are very different, they are calculated separately. If the algorithm is unable to find more than 100 grid points (of either accumulation or ablation) the radius is extended until a threshold of 100 data points for the regression is reached. For simplicity, the local gradients are calculated from the respective pre-industrial SMB simulations. Further details on the SMB gradient method are discussed in Helsen et al. (2012).

Between the SMBs calculated for 130, 125, 120, and 115 ka a linear interpolation is applied, giving a transient SMB forcing over 15,000 years. A more complicated interpolation approach is unnecessary given the smooth climate forcing and the uncertainties related to the Eemian climate and SMB simulations. Plach et al. (2018) give a detailed discussion of the simulated climate evolution and show, for example, an Eemian peak warming of 4-5 °C over Greenland, which is in agreement with proxy reconstructions (NEEM community members, 2013; Landais et al., 2016). The SMBs in the present study (after being corrected for topography) are shown and discussed in Sec. 3.

2.2 The Ice Sheet System Model (ISSM)

The ISSM is a finite-element, thermo-mechanical ice flow model based on the conservation laws of momentum, mass, and energy (Larour et al., 2012) — here model version 4.13 is used (Cuzzone et al., 2018). ISSM employs an anisotropic mesh, which is typically refined by using observed surface ice velocities, allowing fast flowing ice (i.e., outlet glaciers) to be modeled at higher resolution than slow flowing ice (i.e., interior of an ice sheet). Furthermore, ISSM offers inversion methods to ensure that an initialized model matches the observed (modern) ice sheet configuration (i.e., observed ice surface velocities are inverted for basal friction or ice rheology; Morlighem et al., 2010; Larour et al., 2012). While ISSM offers a large range of ice flow representations, in this study the computationally efficient 3D higher-order configuration (Cuzzone et al., 2018) is used. This configuration uses an interpolation based on higher-order polynomials between the vertical layers, instead of the default linear interpolation which requires a much higher number of vertical layers to capture the sharp temperature gradient at the base of an ice sheet. By using a quadratic interpolation, 5 vertical layers are sufficient to capture the thermal structure accurately, while a linear vertical interpolation requires 25 layers to achieve a similar result. This lower number of vertical layers reduces the computational demand for the thermal model and the stress balance calculations, and makes it possible to run 3D higher-order simulations for thousands of years. The simulations over 12,000 years in this study take between 3-4 weeks on a single node with 16 cores.

2.3 Experimental setup

All simulations (forced with MAR-SEB and MAR-BESSI) run from 127 to 115 ka following the Paleoclimate Modeling Intercomparison Project (PMIP4; Otto-Bliesner et al., 2017) experimental design and initiating the Eemian simulations at 127 ka with a modern GrIS. The thermal structure is derived using a thermal steady-state simulation with prescribed pre-industrial temperature at the ice surface (from the regional climate model simulations) and an enthalpy formulation (Aschwanden et al., 2012) at the base to determine the basal conditions (cold or temperate ice). At the base of the ice sheet a prescribed geothermal heat flux (Shapiro and Ritzwoller, 2004) as provided by the SeaRISE dataset (Bindschadler et al., 2013) is imposed. The basal friction coefficients are kept constant over time and are derived from an inversion of spatially varying, observed surface velocities. In this case, an algorithm chooses the basal friction coefficients in a way that the modeled velocities match the observed velocities. In a first inversion, an initial ice viscosity is prescribed. After the thermal steady-state simulation, the ice viscosity is updated as a function of the new thermal profile (Cuffey and Paterson, 2010). In a second inversion, the basal friction coefficients are iterated to minimize three cost functions (Table 1). A map of the basal friction coefficients is provided as a

supplement to this manuscript. The inversion depends on the chosen ice flow approximation due to the different representations of the stress balance. Hence, simulations with the 2D SSA and the 3D higher-order approximations use different inversions.

We use the ISSM default friction law (Larour et al., 2012; Schlegel et al., 2013) based on the empirically derived friction law by Paterson (1994, p. 151):

$$\boldsymbol{\tau_b} = -\alpha^2 \, N_{\text{eff}} \, \boldsymbol{v_b} \tag{1}$$

where $\boldsymbol{\tau_b}$ is the basal shear stress (vector), α the basal friction coefficient (derived by inversion from surface velocities), N_{eff} the effective pressure of the water at the glacier base (i.e., the difference between the overburden ice stress and the water pressure), and $\boldsymbol{v_b}$ the horizontal basal velocity (vector). The effective pressure is simulated with a first order approximation (Paterson, 1994):

$$N_{\text{eff}} = g \, \rho_{\text{ice}} \, H + \rho_{\text{water}} \, z_b \tag{2}$$

where ρ_{ice} and ρ_{water} are the densities of ice and water, respectively, H is the ice thickness, and z_b is the bedrock elevation. From these equations it follows that the initial (modern) basal friction coefficients stay constant, while the basal shear stress evolves over time with the ice thickness and the effective pressure.

Basal sensitivity experiments with changed basal friction are performed to investigate the importance of uncertainties related to basal friction. In order to minimize the number of 3D higher-order experiments, a number of test experiments are performed with the simpler 2D SSA configuration of ISSM to identify the range of basal friction coefficients which yield plausible results. For example, if the basal friction coefficients for the entire ice sheet are reduced by a factor of 0.8 and 0.5 (in the 2D SSA test experiments; not shown), the ice surface elevation at the NEEM location shows a late-Eemian lowering of 300 m and 800 m, respectively. Proxy data indicates a surface lowering of no more than 300 m (NEEM community members, 2013) at this point in time. In order to stay clearly within the proxy reconstructions the friction for the entire ice sheet is reduced by a factor of 0.9 in the 3D higher-order ice flow experiments. Two 2D SSA experiments (forced with MAR-SEB and MAR-BESSI) are discussed in detail here to illustrate the difference of the two ice flow approximations (Table 2). A full list of 2D SSA experiments is given as a supplement to this manuscript.

Due to the high computational demand of the 3D higher-order model, compromises are necessary. The simulations are initiated with the modern GrIS topography and the bedrock remains fixed at modern values (Glacial Isostatic Adjustment; GIA is not yet implemented for transient simulations with ISSM). The ice sheet is initialized with observed ice surface velocities from Rignot and Mouginot (v4Aug2014; 2012). The anisotropic ice sheet mesh is refined with these velocities with a minimum resolution of 40 km in the slow interior and a maximum resolution of 0.5 km at the fast outlet glaciers. Since the mesh is based on observed velocities, the resolution of the mesh remains unchanged over time, and the ice sheet domain is fixed to the present-day ice sheet extent. The ice sheet can freely evolve within this domain, but is unable to grow outside the present-day limits.

Table 1. ISSM model parameters

ISSM model parameters	
minimum mesh resolution (adaptive)	40 km
maximum mesh resolution (adaptive)	0.5 km
number of horizontal mesh vertices	7383
number of vertical layers	5
ice flow approximation	3D higher-order (Blatter, 1995; Pattyn, 2003)
degree of finite elements (stress balance)	P1 x P1
degree of finite elements (thermal)	P1 x P2
minimum time step (adaptive)	0.05 years
maximum time step (adaptive)	0.2 years
basal friction law	Paterson (1994, p. 151); Eq. 1 and 2
basal friction coefficient inversion cost functions	101, 103, 501
ice rheology	Cuffey and Paterson (2010, p. 75)

degree of finite elements: P1 - linear finite elements, P2 - quadratic finite elements, horizontal x vertical; inversion cost functions: 101 - absolute misfit of surface velocities, 103 - logarithmic misfit of surface velocities, 501 - absolute gradient of the basal drag coefficients

The air temperature prescribed at the ice surface remains fixed at pre-industrial levels. Ice formed during the 12,000 year simulations will only reach several hundred meters deep (not reaching the bottom layers which experience most deformation) and surface air temperature is not influencing the SMB (as it would in a degree day model; Reeh, 1989) because SMB is computed by either MAR-SEB or MAR-BESSI, models that account for temperature changes over the Eemian (as simulated by NorESM).

The simplified transient ISSM model configuration does not explicitly resolve processes related to basal hydrology, ocean forcing, and calving. The ice rheology is calculated as a function of temperature following Cuffey and Paterson (2010, p. 75). Initial (modern) ice sheet surface, ice thickness, and bed topography are derived from BedMachine v3 (v2017-09-20; Morlighem et al., 2017). The most important parameters of the ice sheet model are summarized in Table 1. Finally, the shortcomings of this simplified configuration are discussed in Sec. 4.

2.4 Control and sensitivity experiments

The experiments performed are described below and summarized in Table 2. As discussed in Sec. 2.1-2.3, the experiments test the sensitivity to two different SMB models as well as different representations of the basal friction: The *control* experiment applies SMB from MAR-SEB and unchanged (modern) basal friction; the *SMB* experiment tests the simplified, but efficient SMB model, MAR-BESSI; the *basal* experiments test spatially uniform changes to the basal friction for the entire ice sheet; the *outlets* experiments test the sensitivity to changes of basal friction locally at the outlet glaciers (slow down/speed up of outlet

glaciers, defined as high velocity regions with >500 m/yr). For the *basal* and *outlets* experiments the basal friction coefficient is multiplied by factors 0.9 and 1.1. Furthermore, the *outlets* experiments are repeated with more extreme factors of 0.5 and 2.0.

In additional experiments, with the more efficient SSA version of the model, a larger range of basal friction for the entire ice sheet is explored (doubling/halving of basal friction similar to Helsen et al., 2013). However, applying factors of 0.5 and 2.0 for the entire ice sheet results in unrealistic surface height changes at the central Greenland ice core locations (not shown). Therefore, these extreme changes of basal friction are only applied to the outlet glaciers in our 3D higher-order experiments.

The *altitude* experiments test the impact of the SMB-altitude feedback by ignoring this feedback; which means that the transient SMB forcing is prescribed without correcting for altitude changes. Finally, we perform a *relaxed* experiment testing the sensitivity to a larger, relaxed initial ice sheet (with the same SMB and ice dynamics as the *control* experiment). This *relaxed* experiment starts with a larger ice sheet which is spun-up for 10,000 years under constant pre-industrial SMB from MAR-SEB. The difference arising from the different ice flow approximation are illustrated in the *ice flow* experiments.

3 Results

The importance of the SMB forcing is illustrated in Fig. 1 showing the evolution of the Greenland ice volume in the *control* experiment (MAR-SEB; bold orange line) and the *SMB* sensitivity experiment (MAR-BESSI; bold purple line). The corresponding sub-sets of experiments testing the basal friction (*basal*, *outlets*) are indicated in lighter colors. There is a distinct difference between the model experiments forced with the two SMBs: forcing the ice sheet with MAR-SEB SMB (bold orange line) gives a minimum ice volume of 2.73 x 10^{15} m^3 at 124.7 ka corresponding to a sea level rise of 0.5 m — the basal sensitivity experiments give a range of 0.3 to 0.7 m (thin orange lines). On the other hand, the experiments forced with MAR-BESSI (bold purple line) give a minimum of 1.77 x 10^{15} m^3 at 123.8 ka (2.9 m sea level rise) with a range from 2.7 to 3.1 m (thin purple lines). The minimum ice volume and the corresponding sea level rise from all experiments are summarized in Table 3.

The *basal* experiments (thin solid lines; Fig. 1; friction *0.9/*1.1 for the entire ice sheet) show a stronger influence on the ice volume than the *outlets* experiments: changing the basal friction locally at the outlet glaciers (*outlets*) by factors of 0.9 and 1.1 has very little effect on the integrated ice volume (not shown). However, a halving/doubling of the friction at the outlet glaciers does show a notable effect on the ice volume (0.05 to 0.15 m at the ice minimum; thin dashed lines; Fig. 1).

The importance of the SMB-altitude feedback is illustrated in Fig. 2 which shows the evolution of the ice volume with the two SMB forcings (*control*, bold orange; *SMB*, bold purple) and without applying the SMB gradient method (*altitude*, thin orange/purple). Neglecting the correction of the SMB for a changing ice surface elevation, that is using the offline calculated SMBs directly, results in significantly less melt. This is particularly pronounced in experiments forced with MAR-BESSI, because the ablation area in these simulations is larger and therefore larger regions are affected by melt-induced surface lowering. The differences between 3D higher-order and 2D SSA are surprisingly small, particularly at the beginning of the simulations while the ice volume is decreasing (*ice flow*, black and gray). The differences between the ice flow approximations become larger as the ice sheet enters a colder state, at the end of the simulations. Finally, in the *relaxed* experiment (dark green)

Table 2. Overview of the experiments

type of experiment	SMB method	basal friction	ice flow approx.
control	MAR-SEB	modern	3D higher-order
SMB	MAR-BESSI	modern	3D higher-order
basal (reduced)	MAR-SEB	0.9 * modern (entire ice sheet)	3D higher-order
basal (reduced)	MAR-BESSI	0.9 * modern (entire ice sheet)	3D higher-order
basal (enhanced)	MAR-SEB	1.1 * modern (entire ice sheet)	3D higher-order
basal (enhanced)	MAR-BESSI	1.1 * modern (entire ice sheet)	3D higher-order
outlets (reduced)	MAR-SEB	0.5 * modern (outlet glaciers)	3D higher-order
outlets (reduced)	MAR-BESSI	0.5 * modern (outlet glaciers)	3D higher-order
outlets (reduced)	MAR-SEB	0.9 * modern (outlet glaciers)	3D higher-order
outlets (reduced)	MAR-BESSI	0.9 * modern (outlet glaciers)	3D higher-order
outlets (enhanced)	MAR-SEB	1.1 * modern (outlet glaciers)	3D higher-order
outlets (enhanced)	MAR-BESSI	1.1 * modern (outlet glaciers)	3D higher-order
outlets (enhanced)	MAR-SEB	2.0 * modern (outlet glaciers)	3D higher-order
outlets (enhanced)	MAR-BESSI	2.0 * modern (outlet glaciers)	3D higher-order
altitude	MAR-SEB	modern	3D higher-order
altitude	MAR-BESSI	modern	3D higher-order
relaxed	MAR-SEB	modern	3D higher-order
ice flow	MAR-SEB	modern	2D SSA
ice flow	MAR-BESSI	modern	2D SSA

the volume decrease is more pronounced because the relaxed initial ice sheet is larger and the SMB forcing is negative enough to melt the additional ice at the margins. However, at the end of the simulations the *control* and the *relaxed* experiments become indistinguishable.

Comparing the SMB forcing for the *control* experiment (MAR-SEB; Fig. 3a-d) and the *SMB* experiment (MAR-BESSI; Fig. 3e-h) emphasizes the importance of the SMB-altitude feedback. While the offline calculated SMBs (using a modern ice surface) are similar, the surface lowering in combination with the SMB gradient method cause the resulting SMB to become very negative in the southwest (for both MAR-SEB and MAR-BESSI) and in the northeast (particularly for MAR-BESSI). Regions with extremely low SMB at 125 ka are ice-free at the time of the simulation (ice margins are indicated with a black solid line).
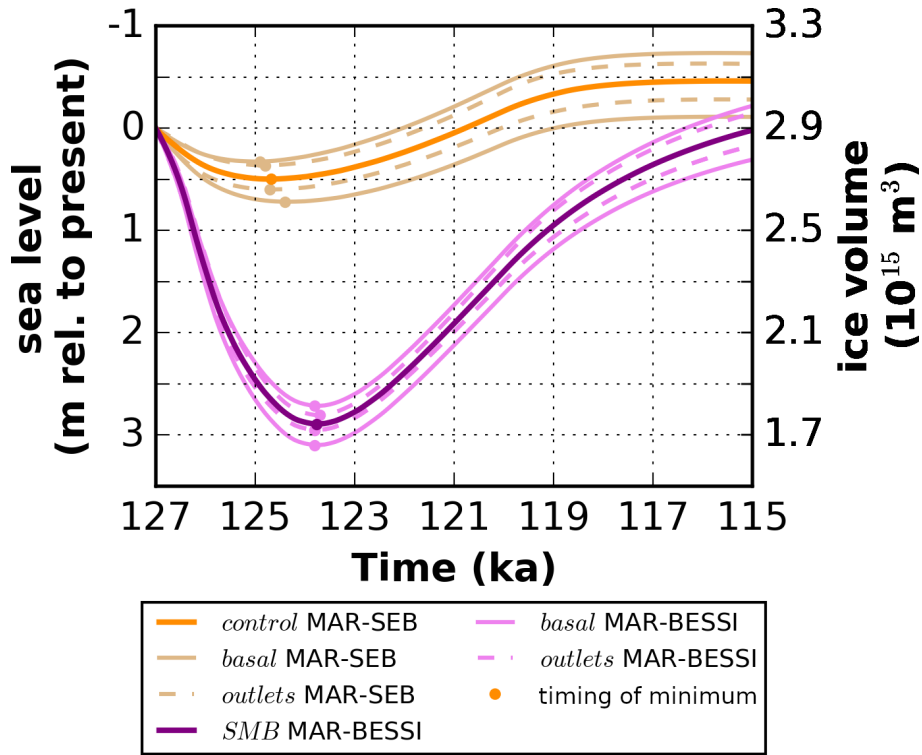
Figure 1. Evolution of the ice volume for the *control* (MAR-SEB, orange, bold) and the *SMB* (MAR-BESSI, purple, bold) experiments in comparison with the *basal/outlets* sensitivity experiments. The *basal* (friction *0.9/*1.1 for the entire ice sheet) and *outlets* sensitivity experiments (friction *0.5/*2.0 at the outlet glaciers) are indicated with thin solid and thin dashed lines, respectively. Note that the lower friction experiments give lower volumes. The minimum of the respective experiments is indicated with circles. See Table 3 for the exact values.

The simulated ice sheet thickness in the *control* experiment (Fig. 4a-d; MAR-SEB) shows only moderate changes. However, there is a significant retreat of the ice margin in the southwest at 125 ka (Fig. 4b). The *SMB* sensitivity experiment (Fig. 4e-h; MAR-BESSI) on the other hand gives a very different evolution of the ice thickness: At 125 ka the *SMB* experiment (Fig. 4f) shows an enhanced retreat in the southwest, and additionally a particularly strong retreat in the northeast. Furthermore, the ice

5 sheet takes longer to recover in the *SMB* experiment, giving a smaller ice sheet at 120 ka (Fig. 4g), mainly due to the large ice loss in the northeast.

The MAR-SEB forced experiments give only small changes (±200 m) in ice surface elevation at the ice core locations of Camp Century, NEEM, NGRIP, GRIP, Dye-3, and EGRIP (Fig. 5). At most locations the surface elevation increases due to a positive SMB, which is not in equilibrium with the initial ice sheet. The *relaxed* experiment (dark green), which is in

10 equilibrium with the initial climate, shows damped elevation changes. Notably, Dye-3 (Fig. 5c) shows the strongest initial lowering due to its southern location affected by the early Eemian warming. The MAR-BESSI-forced experiments show the largest changes in surface elevation, particularly at Dye-3 (Fig. 5c) and NGRIP (Fig. 5b) with a maximum lowering of around
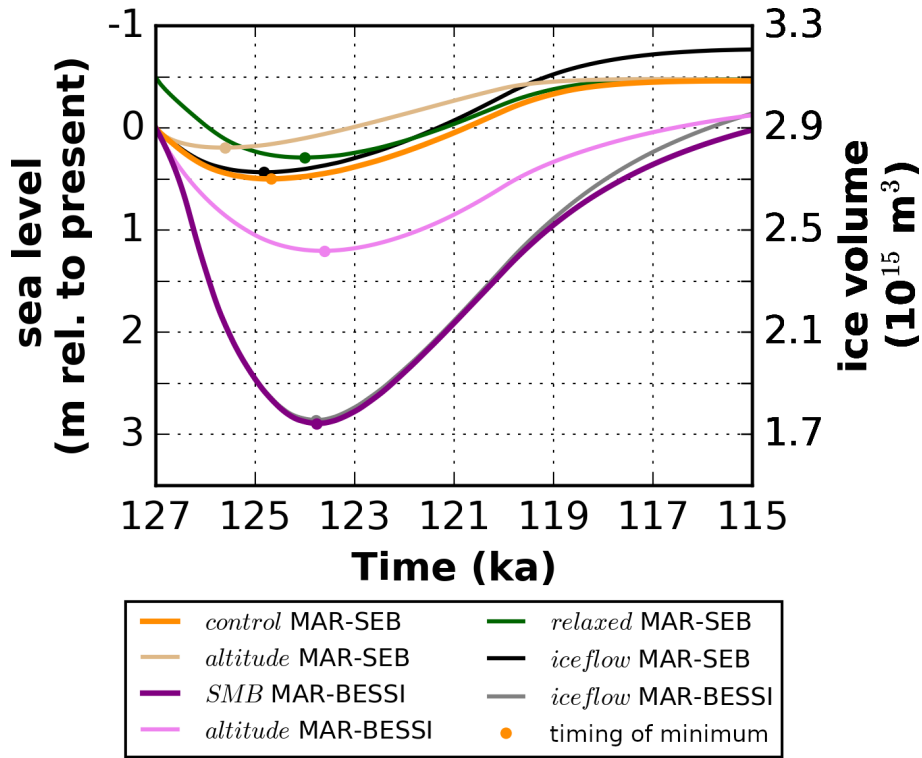
Figure 2. Evolution of the ice volume for the *control* (MAR-SEB, orange, bold) and the SMB experiments (MAR-BESSI, purple, bold) in comparison with the *altitude*, *relaxed*, and *iceflow* sensitivity experiments. The corresponding *altitude* (no SMB-altitude feedback) and *iceflow* (2D SSA) sensitivity experiments are shown in lighter colors and black/gray, respectively. The *relaxed* sensitivity experiment (relaxed larger initial ice sheet, but otherwise *control* forcing) is shown in dark green.

600 m, and at EGRIP (Fig. 5f), where the the largest lowering is around 1500 m. In contrast to the ice volume evolution, where differences between the *control* and the *ice flow* experiment are small (Fig. 2), there is a larger difference in ice surface elevation changes between the ice flow approximations. The 2D SSA experiments (Fig. 5, black and grey) show ice surface changes up to 200 m different from the 3D higher-order experiments (Fig. 5, bold orange and purple).

5   The impact of all sensitivity experiments on the ice volume minimum is summarized in Fig. 6. The choice of SMB model (*SMB*, black) shows the strongest influence with a difference in sea level rise of ~2.5 m between the *control* experiment (with MAR-SEB) and the *SMB* experiment (with MAR-BESSI). Furthermore, the SMB-altitude feedback is particularly important for the MAR-BESSI forced *altitude* experiment, due to the large regions affected by melt-induced surface lowering. The *basal* and *outlets* sensitivity experiments show a limited effect on the simulated ice volume minimum. Finally, using a larger, relaxed

10   initial ice sheet (*relaxed*) results in a ~0.3 m larger sea level rise. A complete summary of the respective ice volume minima is given in Table 3.
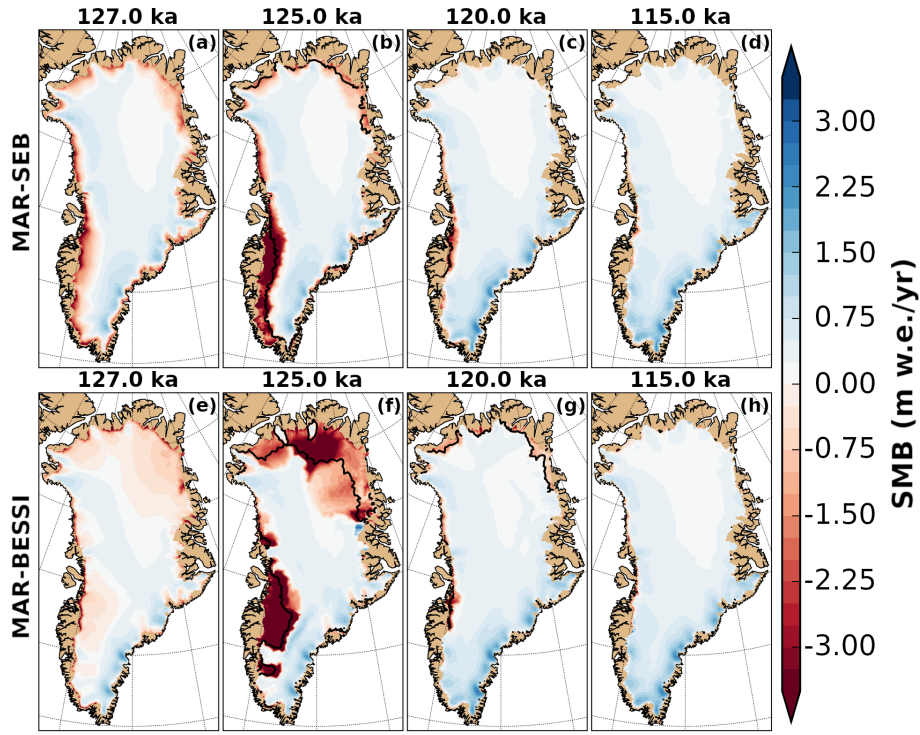
Figure 3. SMB forcing corrected for surface elevation changes at 127, 125, 120, 115 ka for the *control* (a-d, MAR-SEB) and the *SMB* (e-h, MAR-BESSI) experiments. The ice margin is indicated with a solid black line (10 m ice thickness remaining). A nonvisible ice margin is identical with the domain margin. For a consistent comparison, the SMB is shown at 125 ka instead of the individual minimum (*control* at 124.7 ka and *SMB* at 123.8 ka).

There are small differences between the simulated ice thickness minimum of the *control* experiment (Fig. 7a; MAR-SEB and 3D higher-order) and the corresponding *ice flow* experiment (Fig. 7b; MAR-SEB and 2D SSA). Only minor differences are visible on the east coast, where the 2D SSA experiment shows a stronger thickening than the 3D higher-order experiment.

Reducing the friction at the base of the entire ice sheet by a factor of 0.9 (*basal**0.9, Fig. 8b) results in a thinning on the order
5 of 100 m in large parts of the ice sheet relative to the ice sheet minimum in the *control* experiment (Fig. 8a). The faster flowing ice sheet leads to a build up of ice at the margins and the topographically constrained outlet glaciers, particularly visible in the northeast. In contrast, reducing the basal friction only at the outlet glaciers by a factor of 0.5 (*outlets**0.5 Fig. 8c), leads to a regional thinning of several hundred meters focused around the outlet glaciers. Note that the thinning also affects ice thickness upstream from the outlet region.

10 The ice velocities in the $basal$*0.9 experiments indicate that a Greenland-wide reduction of basal friction by a factor of 0.9 leads to a speed up of the outlet glaciers by up to several 100 m/year (Fig. 9b) relative to the *control* experiment. Furthermore, reducing the friction at the outlet glaciers by a factor of 0.5 (*outlets**0.5) results in a regional speed-up of several 100 m/yr (Fig. 9c). Although the $outlets$*0.5 experiment also shows a speed-up further upstream (in the order of several m/yr), in
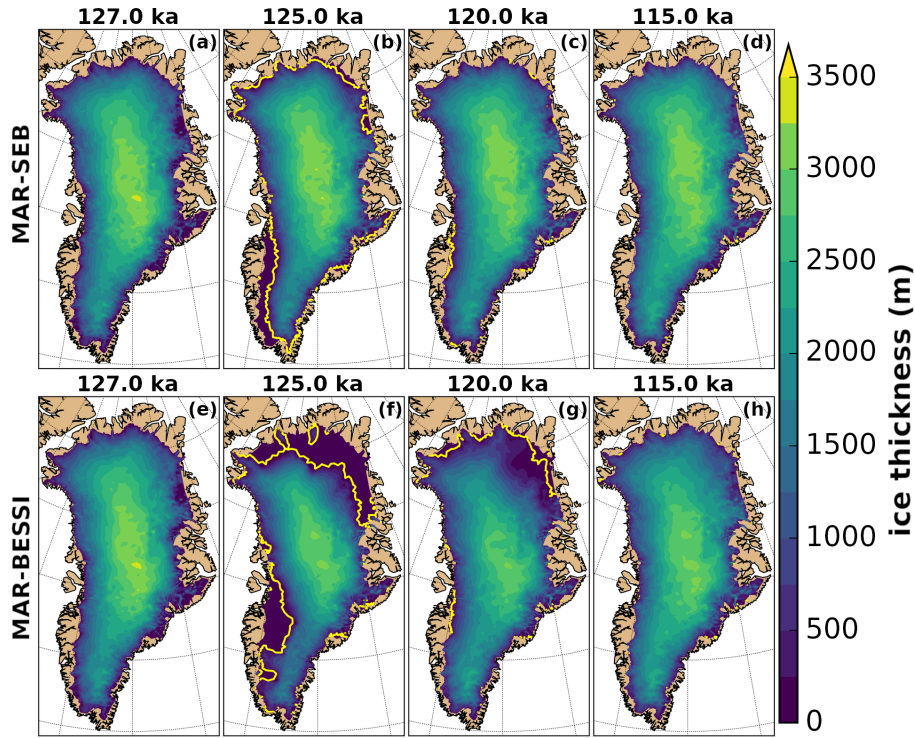
Figure 4. Ice thickness at 127, 125, 120, 115 ka for the *control* (a-d, MAR-SEB) and the *SMB* (e-h, MAR-BESSI) experiments. The ice margin is indicated with a solid yellow line (10 m ice thickness remaining). A nonvisible ice margin is identical with the domain margin. For a consistent comparison, the ice thickness is shown at 125 ka instead of the individual minimum (*control* at 124.7 ka and *SMB* at 123.8 ka).

combination with the local ice thinning (Fig. 8c), the effects of halving the friction at the outlet glaciers shows a minimal effect on the total ice volume (see also in Fig. 1).

4   Discussion

Changing the SMB forcing — between a full surface energy balance model (MAR-SEB) and an intermediate complexity
5   SMB model (MAR-BESSI) — gives the largest difference in our simplified simulations of the Eemian ice sheet evolution (Fig. 6). Compromises such as the lack of ocean forcing and GIA, and limited changes of basal friction are necessary to keep 3D higher-order millennial-scale simulations feasible and are discussed in this section.

MAR-SEB and MAR-BESSI are two estimates of Eemian SMBs selected from a wider range of simulations analyzed in Plach et al. (2018). The same Eemian global climate simulations from NorESM, downscaled over Greenland with the regional
10   climate model MAR, are used as forcing for the SMB models. Since only one global climate model is used in this study, uncertainties related to the Eemian climate cannot be evaluated here. Instead the reader is referred to the discussion in Plach et al. (2018).
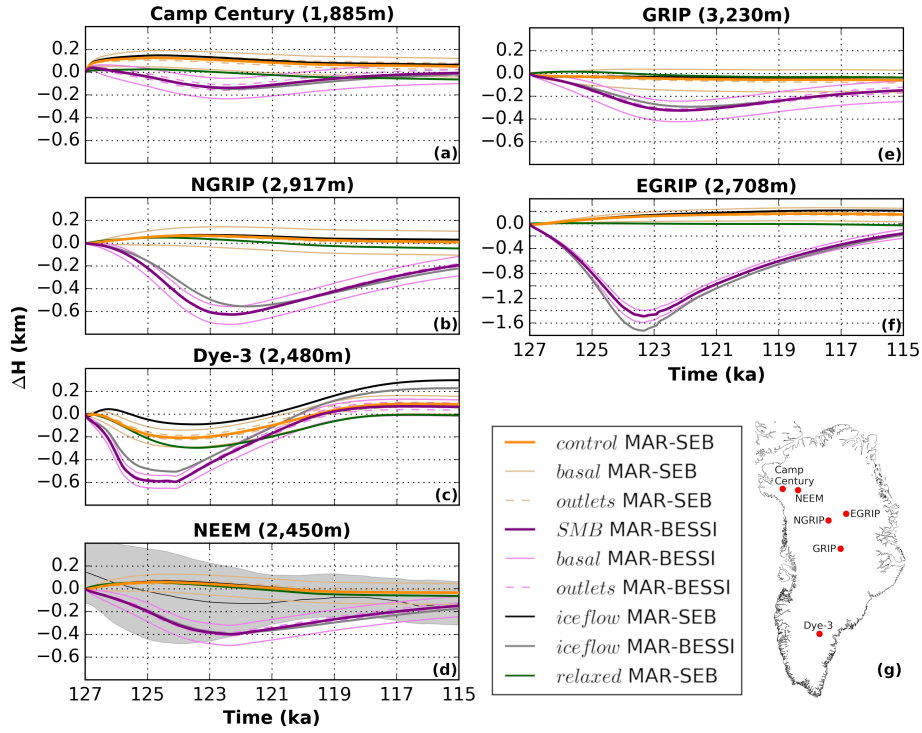
Figure 5. Ice surface evolution at Greenland ice core locations for the *control*, *SMB*, *basal*, *outlets*, *ice flow*, and *relaxed* experiments — Camp Century, NEEM, NGRIP, GRIP, and Dye-3 are shown on the same scale; EGRIP is shown on a different scale. Same color-coding as in Figs. 1 and 2. Surface elevation reconstructions from total gas content at NEEM are indicated with gray shading. Note that the 2D experiments are plotted in the background and therefore hardly visible in some cases, particularly at NEEM.

Our *control* experiment with the 3D higher-order ice flow model with modern, unchanged basal friction coefficients, and forced with MAR-SEB SMB shows minor melting (equivalent to 0.5 m sea level rise), while the *SMB* sensitivity experiment with MAR-BESSI SMB causes a much larger ice sheet retreat (2.9 m sea level rise; Fig. 1). The basal sensitivity experiments (*basal/outlets*) give an uncertainty of ±0.2 m sea level rise on top of the SMB simulations (Fig. 1); with the Greenland-wide

5   basal friction change (*basal*) showing the largest influence on the minimum ice volume. Reducing/enhancing the friction at the outlet glaciers (*outlets*) by a factor of 0.9/1.1 shows mainly local thinning/thickening at the outlets (Fig. 8c) with limited effect on the total ice volume (Fig. 1, Table 3). However, doubling the friction at the outlet glaciers reduces the sea level rise contribution by 0.15 and 0.10 m for MAR-SEB and MAR-BESSI SMB forcing, respectively (relative to the *control* experiment; Table 3).

10   The basal friction sensitivity experiments (*basal/outlets*) are non-exhaustive and further experiments could be envisioned, including a lower velocity threshold to define the outlet glaciers, continuous identification of outlet regions, and combining *basal**0.9 and *outlets**0.5 experiments. In such experiments the impact on the ice sheet evolution might be larger than in the experiments discussed. Regardless of the specific formulation of the anomalous basal friction, the sensitivity experiments

Table 3. Summary of the simulated ice sheet minima for all experiments

experimental setup	SLR [m] rel. to initial	ΔSLR [m] at resp. minimum	Minimum GrIS volume (10^{15}m^3)
control **MAR-SEB**	**0.51**	**0.00**	**2.73**
basal*0.9 MAR-SEB	0.73	+0.22	2.64
basal*1.1 MAR-SEB	0.33	-0.17	2.80
outlets*0.5 MAR-SEB	0.61	+0.10	2.69
outlets*0.9 MAR-SEB	0.53	+0.02	2.72
outlets*1.1 MAR-SEB	0.48	-0.02	2.74
outlets*2.0 MAR-SEB	0.36	-0.15	2.79
altitude MAR-SEB	0.18	-0.32	2.86
relaxed MAR-SEB	0.79	+0.28	2.82
ice flow (2D) MAR-SEB	0.43	-0.07	2.76
SMB MAR-BESSI	2.90	0.00	1.77
basal*0.9 MAR-BESSI	3.10	+0.20	1.69
basal*1.1 MAR-BESSI	2.72	-0.18	1.84
outlets*0.5 MAR-BESSI	2.95	+0.05	1.75
outlets*0.9 MAR-BESSI	2.90	+0.00	1.77
outlets*1.1 MAR-BESSI	2.87	-0.03	1.78
outlets*2.0 MAR-BESSI	2.80	-0.10	1.81
altitude MAR-BESSI	1.20	-1.70	2.45
ice flow (2D) MAR-BESSI	2.85	-0.05	1.79

For the *outlets* sensitivity experiments, the basal friction in regions with > 500 m/yr is changed. Sea level rise (SLR) values are relative to the initial ice sheet at 127 ka, i.e., the modern ice sheet for all experiments except the relaxed initial ice sheet experiment. The lost ice volume is equally spread over the modern ocean area. ΔSLR refers to anomalies relative to the respective SMB forcing experiments with unchanged friction.

shown here represent a substantial change in basal properties and they illustrate the magnitude of the uncertainties related to the basal conditions implying that caution is required when deriving the basal friction. Finding appropriate basal conditions of past ice sheets is challenging. We show that after applying a large range of frictions it is unlikely that friction at the base has a stronger influence than changing the SMB forcing. This might be different if sub-glacial hydrology fed by SMB is dynamically included.
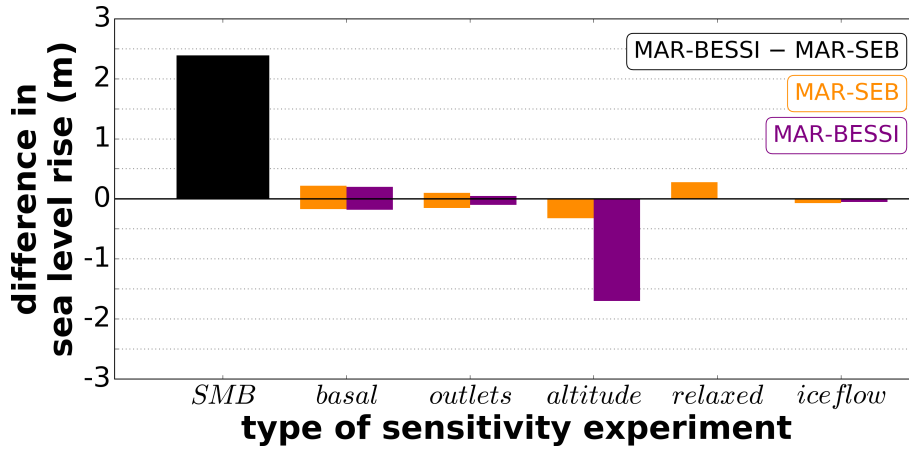
Figure 6. Differences between the minimum Eemian ice sheet simulated by the respective sensitivity experiments: *SMB* (black): difference between the *control* and the *SMB* experiment (MAR-SEB and MAR-BESSI, respectively). *basal*: experiments with changed friction for the entire ice sheet. *outlets*: experiments with changed friction at the outlet glaciers. *altitude*: experiments without the SMB-altitude feedback. *relaxed*: experiment with a larger, relaxed initial ice sheet. *ice flow*: experiments with 2D SSA instead of the default 3D higher-order ice flow approximation. The different SMB forcing is shown in orange (MAR-SEB) and purple (MAR-BESSI). *basal/outlets* experiments show positive and negative values because they are performed with enhanced and reduced friction. The exact values are given in Table 3.

The importance of coupling climate (SMB) and ice sheet has been demonstrated in previous studies, e.g., recently for regional climate models in a projected future climate assessment by Le clec'h et al. (2019). However, running a high resolution regional climate model over several thousand years is presently unfeasible due to the exceedingly high computational cost. This is even more true when the goal is to run an ensemble of long sensitivity simulations as presented here. Although the presented simulations are lacking the ice-climate coupling, the SMB-altitude feedback is accounted for by applying the SMB gradient method. The SMB is significantly lowered as the ice surface is lowered: neglecting the SMB-altitude feedback gives less than half the volume reduction (MAR-SEB: 0.2 vs. 0.5 m; MAR-BESSI: 1.2 vs. 2.9 m; Figs. 2 and 6).

Towards the end of the simulations, all model experiments develop a new ice sheet state which is larger than the initial state (Figs. 1 and 2). This development towards a larger ice sheet is likely related to a relaxation of the initial pre-industrial ice sheet (initial ice sheet is not in equilibrium with the initial SMB forcing) and the colder-than-present 115 ka climate. A simulation over 10,000 years with constant pre-industrial SMB gives a ~10% larger relaxed modern ice sheet. The *relaxed* sensitivity experiments with this relaxed initial ice sheet (~0.5 m global sea level equivalent larger initial state) result in a ~0.3 m larger sea level rise (at the minimum) compared to the *control* experiment. Although the 127 ka GrIS is not expected to be in equilibrium with pre-industrial forcing, the *relaxed* experiment demonstrates the impact of a larger initial ice sheet on our estimates of the contribution of Greenland to the Eemian sea level high-stand. Furthermore, the *relaxed* experiment illustrates the strong, but slow, impact of the SMB forcing. Even when starting with a different initial ice sheet configuration, the final size is similar to the *control* experiment, because late-Eemian SMB results in a steady-state of the ice sheet.
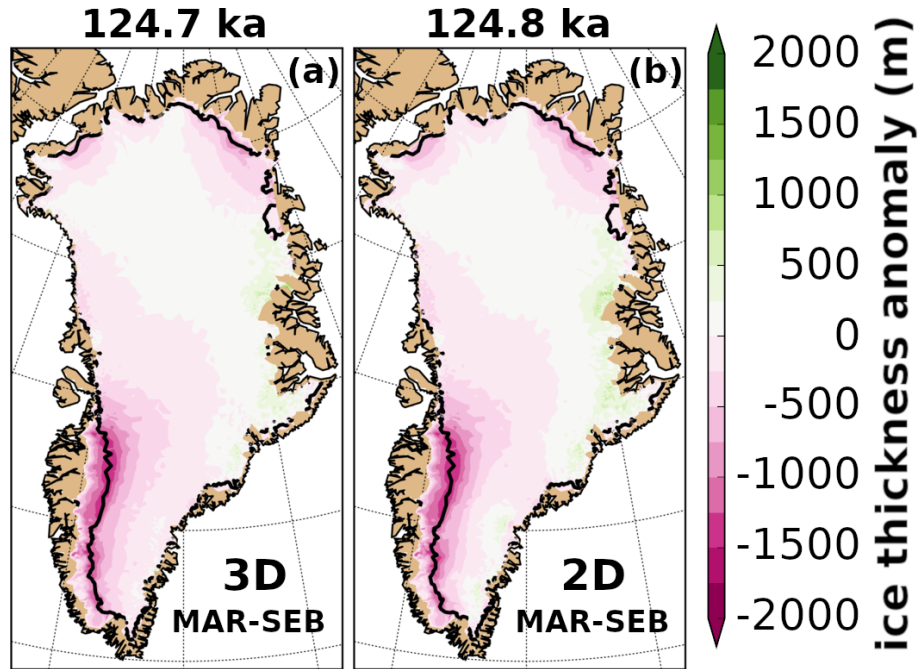
Figure 7. Ice thickness anomalies simulated with the *control* (a; 3D higher-order) and the *ice flow* (b; 2D SSA) experiments at the respective ice minimum. Anomalies are relative to the initial, modern ice sheet. The respective minimum time is indicated on the top of each panel. The ice margin is indicated with a solid black line (10 m ice thickness remaining). If the ice margin is not visible it is identical with the domain margin.

Furthermore, the simplified initialization implies that the thermal structure of the simulated ice sheet is lacking the history of a full glacial-interglacial cycle, i.e., the ice rheology of our ice sheet is different to an ice sheet which is spun-up through a glacial cycle. Helsen et al. (2013) demonstrate the importance of the ice rheology for the pre-Eemian ice sheet size. They find differences of up to 20% in initial ice volume after a spin-up forced with different glacial temperatures (in simulations

5 with basal conditions not based on assimilation of surface velocities as it is the case here). In our approach a biased thermal structure is partly compensated by basal friction optimized so that the simulated surface velocities represent the observed, modern velocities. A viable way to test the influence of the thermal structure on the ice rheology would be to perform additional sensitivity experiments using a 3D higher-order model (the 2D SSA setup neglects vertical shear).

Starting the simulations with a smaller ice sheet would influence the simulated maximum sea level contribution. A smaller

10 ice sheet, in combination with the SMB-altitude feedback, would result in a more negative SMB at the lower surface regions. This could potentially lead to smaller differences between the MAR-SEB and MAR-BESSI results because large regions in the MAR-BESSI simulations melted away completely, and a more negative SMB would show limited effect in such regions. However, the MAR-SEB simulations are more likely to be affected by the lower initial ice elevation. Note that, neglecting GIA
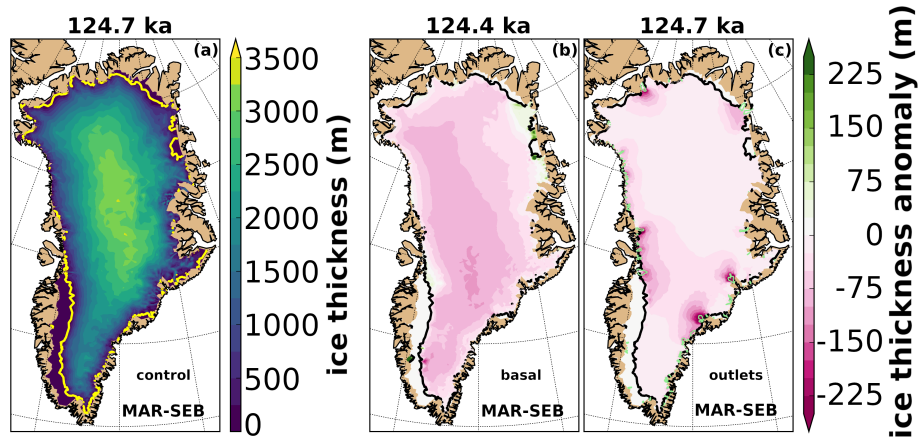
Figure 8. Ice thickness of the *control* experiment (a), the *basal**0.9 (b; reduced friction of the entire ice sheet), and the *outlets**0.5 (c; reduced friction at outlet glaciers) experiments at their respective ice sheet minimum (time indicated on top of panels). Anomalies are relative to the *control* experiment. The ice margin is indicated with a solid yellow/black line (10 m ice thickness remaining). If the ice margin is not visible it is identical with the domain margin. The outlet regions are indicated with bright green contours (c).
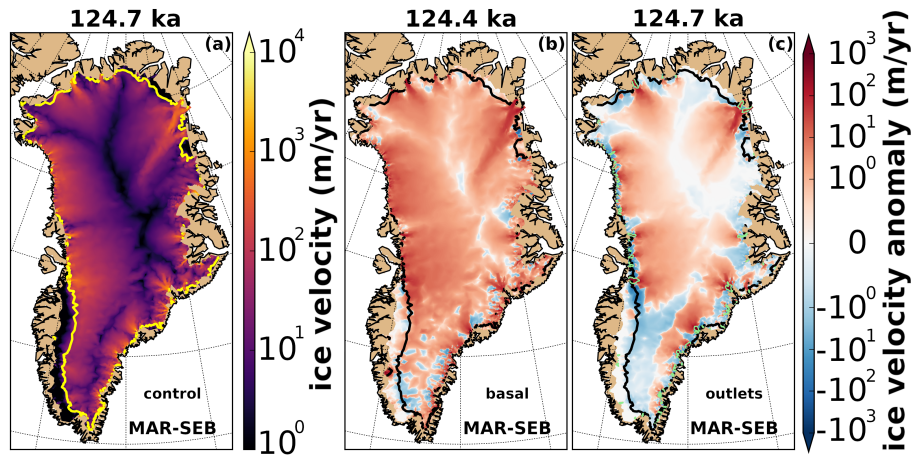
Figure 9. Ice velocity of the ice sheet in the *control* experiment (a) and the *basal**0.9 (b; reduced friction of the entire ice sheet), and the *outlets**0.5 (c; reduced friction at outlet glaciers) experiments at their respective ice sheet minimum (time indicated on top of panels). Anomalies are relative to the *control* experiment. The ice margin is indicated with a solid yellow/black line (10 m ice thickness remaining). If the ice margin is not visible it is identical with the domain margin. The outlet regions are indicated with bright green contours (c).

could counteract the effect of a lower initial ice sheet as well as a negative SMB, as the isostatic rebound of the regions affected by melt would partly compensate for the height loss.

The *ice flow* experiments (2D SSA) show very similar results to the corresponding experiments with 3D higher-order (*control* and *SMB* experiments; Fig. 7). The minor differences in the east, a stronger thickening in the 2D SSA experiments, might be

explained by the complex topography in this region. The differences in ice volume between 3D higher-order and 2D SSA experiments (Fig. 2) become larger towards the end of the simulations under colder climate conditions (less negative SMB). Furthermore, the ice surface evolution at the ice core locations show a similar behavior with both ice flow approximations, differences are less than ~150 m (at most locations). The strong similarities between 3D higher-order and 2D SSA, also noted

5 by Larour et al. (2012) using ISSM for centennial simulations, are likely related to the inversion of the friction coefficients from observed velocities. The dynamical deficiencies of the 2D SSA ice flow are partly compensated by the inversion algorithm. This algorithm chooses basal conditions such that the model simulates surface velocities as close to the observations as possible. The relatively small difference between the 3D higher-order and 2D SSA experiments emphasize the controlling role of the SMB forcing and the SMB-altitude feedback in our simulations. However, ice flow induced thinning (for example due to increased

10 basal sliding) could initiate or enhance the SMB-altitude feedback.

Basal hydrology is neglected in the simulations because it is not well understood and therefore difficult to implement in a robust way. However, it is recognized that basal hydrology might have been important for the recent observed acceleration of Greenland outlet glaciers (e.g., Aschwanden et al., 2016). Therefore, the impact of changing basal conditions is tested by varying the friction at the bed of the outlet glaciers. Although basal hydrology is not explicitly simulated, its possible

15 consequences in form of a slow down, or speed-up of the outlet glaciers is assessed (Figs. 8 and 9).

The focus of this study is on the minimum Eemian ice sheet which has likely been land-based. Our Greenland-wide simulations neglect ocean forcing and processes such as grounding line migration. Although ocean interaction is deemed an important process for marine-termination glaciers in observations (Straneo and Heimbach, 2013), a recent study presenting ocean forcing sensitivity experiments for the Eemian GrIS indicates that the Eemian minimum is governed by the atmospheric forcing, due to

20 a lack of ice-ocean contact (Tabone et al., 2018). In contrast, the size of the glacial pre-Eemian ice sheet in their simulations is strongly influenced by the ocean heat flux and submarine melting parameter choice, implying a large impact of ocean forcing on the magnitude of ice loss over the transition into the Eemian. Our simulations, however, are initiated at 127 ka with the observed modern GrIS geometry, not with a large glacial ice sheet (following the PMIP4 protocol; Otto-Bliesner et al., 2017). Similar to Tabone et al. (2018) we therefore do not expect our smaller-than-present Eemian minimum ice sheet to be strongly

25 sensitive to ocean forcing and conclude that the disregard of ocean forcing and processes such as grounding line migration only represents a negligible error in the magnitude of ice loss and our sea level rise estimates.

The choice of starting the simulations with the observed modern GrIS geometry is based on the fact that the present-day ice sheet is relatively well known whereas the configuration of the pre-Eemian ice sheet is highly uncertain. Since global sea level went from a glacial low-stand to an interglacial high-stand, during the course of the Eemian interglacial period, it is a fair

30 assumption that the Eemian GrIS, at some point during this transition, resembled the present-day ice sheet. In this study, this point is chosen to be at 127 ka. One advantage of this initialization procedure, is that it allows for a basal friction configuration based on inverted observed modern surface velocities. A spin-up over a glacial cycle without adapting basal friction would be unrealistic. Furthermore, a spin-up would require ice sheet boundary migration, i.e., implementation of calving, grounding line migration, and a larger ice domain. This would be challenging as the mesh resolution is based on observed surface velocities

35 and the domain therefore limited to the present-day ice extent. Additionally, a time-adaptive mesh, to allow for the migration
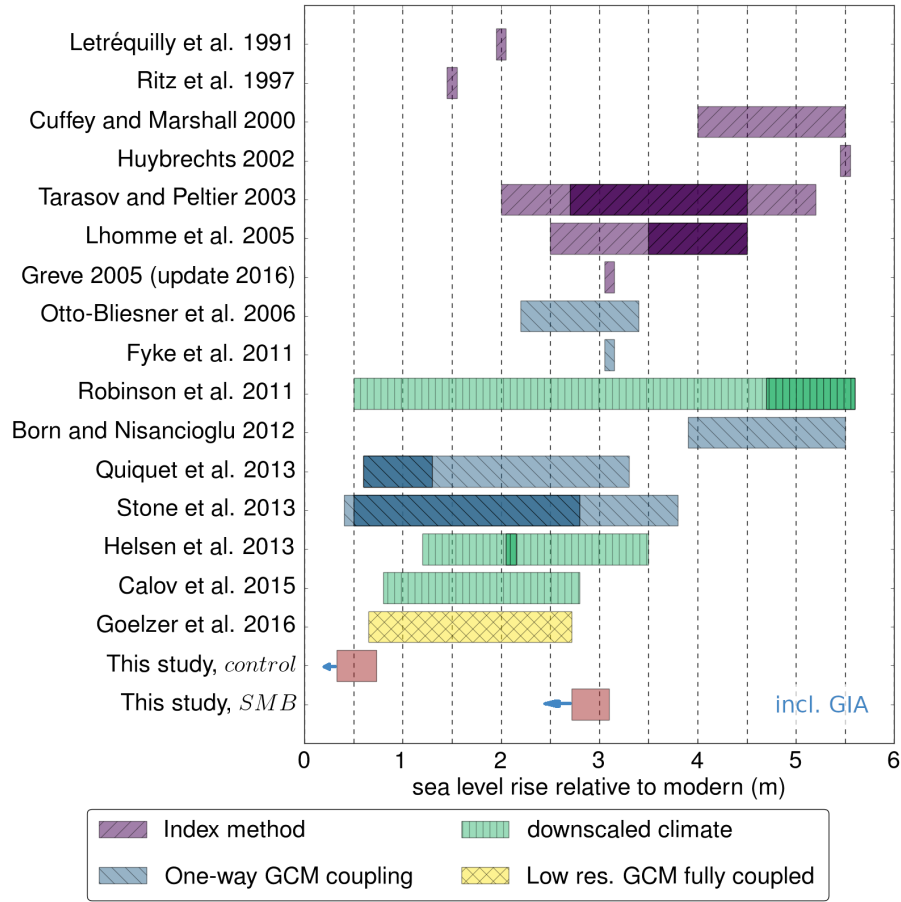
Figure 10. Simulated sea level rise contributions from this study and previous Eemian studies. For this study the results of the *control* (MAR-SEB; lower bound) and the *SMB* experiments (MAR-BESSI; upper bound) are shown (the ranges show the results of the respective basal/outlets fraction sensitivity experiments). Previous studies are color-coded according to the type of climate forcing used. More likely estimates are indicated with darker colors if provided in the respective studies. A common sea level rise conversion (distributing the meltwater volume equally on Earth's ocean area) is applied to Greve (2005), Robinson et al. (2011), Born and Nisancioglu (2012), Quiquet et al. (2013), Helsen et al. (2013), and Calov et al. (2015). Tendencies of a GIA inclusion are indicated by blue arrows. The simulations of Greve (2005) were repeated with an updated ice sheet model version in 2016 (personal communication).

of the high resolution mesh with the evolving ice streams, would be necessary. Unfortunately, a realistic spin-up with all these additions is presently unfeasible due to the high computational cost of the model. Moreover, the lack of a robust estimate of the pre-Eemian GrIS size and the climate uncertainties over the last glacial cycle would introduce many more uncertainties to the initial ice sheet configuration.

5   The Eemian GrIS sea level contribution of ~0.5 m in the *control* experiment is low compared to previous Eemian model studies (Fig. 10). Proxy studies based on marine sediment cores (Colville et al., 2011) and ice cores (NEEM community members,

2013) provide a sea level rise estimate of 2 m from the Greenland ice sheet during the Eemian, while assuming no contribution from the northern part of the ice sheet where no proxy constraints are available. However, scenarios with larger contributions from the North could be possible as in the MAR-BESSI forced experiments. Although the *SMB* sensitivity experiment forced with SMB from MAR-BESSI shows a larger global sea level contribution of ~3.0 m, which is closer to previous model esti-
5 mates, this does not necessarily mean that the MAR-BESSI SMB is more realistic. The low sea level contribution of the *control* experiment could indicate systematic biases in the experimental setup, causing a general underestimation of the Eemian sea level contribution in all simulations.

No GIA processes are currently included in the transient mode of ISSM. However, including rebound of the solid Earth would have the tendency to counteract the surface melting. Especially, the MAR-BESSI experiments are affected by considerable
10 melt-induced surface lowering. The solid Earth responds in time-scales of several thousand years, and therefore can oppose part of the extreme surface lowering during the warmest part of the Eemian, resulting in a reduced GrIS contribution to global sea level rise. The MAR-SEB experiments show less extensive melting and less surface lowering and as a result the potential for GIA to influence the MAR-SEB SMBs is smaller. The tendencies of how the sea level rise estimates could be influenced by an inclusion of GIA are indicated by blue arrows in Fig. 10.

15 Both SMB models are forced with a regionally downscaled climate based on simulations with the global climate model NorESM. NorESM, as other climate models, has biases, which end up in the SMBs through downscaling procedures. This present study can be seen as a sensitivity study to SMB forcing for millennial-scale ice sheet simulations. While the simplified setup has its limits, the study emphasizes the importance of the accurate SMB forcing in general, independent on how well the presented SMBs describe the Eemian SMB. Furthermore, it is important to keep in mind that an accurate SMB forcing not
20 only depends on the choice of SMB model, but also the climate simulations used as input.

5   Conclusions

This study emphasizes the importance of an accurate surface mass balance (SMB) forcing over a more complex ice flow approximation for the simulation of the Greenland ice sheet during the Eemian. Experiments with two SMBs — a full surface energy balance model and an intermediate complexity SMB model — result in different Eemian sea level contributions
25 (~0.5 to 3.0 m) when forced with the same detailed regional climate over Greenland. In contrast, the comparison of experiments with 3D higher-order and 2D SSA ice flow, give only small differences in ice volume (<0.2 m). Furthermore, the importance of the SMB-altitude feedback is shown; neglecting this feedback reduces the simulated sea level contribution by more than 50%. A non-exhaustive set of basal friction sensitivity experiments, affecting the entire ice sheet and only the outlet glacier regions, indicate their limited influence on the total ice volume (maximum difference of ~0.2 m compared to experiments with
30 default friction). While basal friction sensitivity experiments with larger impacts on the ice configuration could be envisioned, it is unlikely that such experiments would exceed the magnitude of uncertainty related to SMB. While it is challenging and arguably unfeasible at present to perform an exhaustive set of sensitivity experiments with 3D higher-order ice flow models,

cost-efficient hybrid models (SIA + SSA) could be an option to further investigate the ice dynamical processes (such as ocean forcing or basal hydrology) neglected here.

In conclusion, simulations of the long-term response of the Greenland ice sheet to warmer climates, such as the Eemian interglacial period, should focus on an accurate SMB estimate. Moreover, it is important to note that uncertainties in SMB are not only a result of the choice of SMB model, but also the climate simulations used as input. Climate model uncertainties and biases are neglected in this study. However, they should be included in future Eemian ice sheet model studies in an effort to provide reliable estimates of the Eemian sea level contribution from the Greenland ice sheet.

6 Code availability

The ISSM code can be freely downloaded from http://issm.jpl.nasa.gov (last accessed: 18.10.2018). Model scripts and other datasets can be obtained upon request from the corresponding author. The NorESM model code can be obtained upon request. Instructions on how to obtain a copy are given at: https://wiki.met.no/noresm/gitbestpractice (last accessed: 18.10.2018). The source code for BESSI is available as a supplement to Born et al. (2019). The MAR code is available at: http://mar.cnrs.fr (last accessed: 18.10.2018).

7 Data availability

The ISSM simulations and the MAR-SEB and MAR-BESSI SMBs are available upon request from the corresponding author. The SeaRISE dataset used is freely available at: http://websrv.cs.umt.edu/isis/images/e/e9/Greenland_5km_dev1.2.nc. (last accessed: 18.10.2018)

Author contributions. AP and KHN designed the study with contributions from PML and AB. SLC performed the MAR simulations. AP performed the ISSM simulations, made the figures and wrote the text with input from KHN, PML, AB, SLC.

Competing interests. The authors declare that they have no conflict of interest.

Acknowledgements. The research leading to these results has received funding from the European Research Council under the European Community's Seventh Framework Programme (FP7/2007-2013) / ERC grant agreement 610055 as part of the ice2ice project. The simulations were performed on resources provided by UNINETT Sigma2; the National Infrastructure for High Performance Computing and Data Storage in Norway (NN4659k; NS4659k). The publication of this manuscript was supported by the open access funding of the University of Bergen. PML was supported by the RISES project of the Centre for Climate Dynamics at the Bjerknes Centre for Climate Research. SLC acknowledges the financial support from the French–Swedish GIWA project, the ANR AC-AHC2, as well as the iceMOD project funded by the Research Foundation – Flanders (FWO-Vlaanderen). We thank J. K. Cuzzone for assisting in setting up the higher-order ISSM runs, M. M. Helsen for helping with the SMB gradient method, and B. de Fleurian for helping to resolve technical issues with ISSM. Furthermore,

we very much thank Bas de Boer, an anonymous referee, and the editor Arjen Stroeven for their comments which significantly improved this manuscript.

References

Aschwanden, A., Bueler, E., Khroulev, C., and Blatter, H.: An enthalpy formulation for glaciers and ice sheets, Journal of Glaciology, 58, 441–457, https://doi.org/10.3189/2012JoG11J088, 2012.

Aschwanden, A., Fahnestock, M. A., and Truffer, M.: Complex Greenland outlet glacier flow captured, Nature Communications, 7, 10 524, https://doi.org/10.1038/ncomms10524, 2016.

Bindschadler, R. A., Nowicki, S., Abe-Ouchi, A., Aschwanden, A., Choi, H., Fastook, J., Granzow, G., Greve, R., Gutowski, G., Herzfeld, U., Jackson, C., Johnson, J., Khroulev, C., Levermann, A., Lipscomb, W. H., Martin, M. A., Morlighem, M., Parizek, B. R., Pollard, D., Price, S. F., Ren, D., Saito, F., Sato, T., Seddik, H., Seroussi, H., Takahashi, K., Walker, R., and Wang, W. L.: Ice-sheet model sensitivities to environmental forcing and their use in projecting future sea level (the SeaRISE project), Journal of Glaciology, 59, 195–224, https://doi.org/10.3189/2013JoG12J125, 2013.

Blatter, H.: Velocity and stress fields in grounded glaciers: a simple algorithm for including deviatoric stress gradients, Journal of Glaciology, 41, 333–344, https://doi.org/10.3189/S002214300001621X, 1995.

Born, A. and Nisancioglu, K. H.: Melting of Northern Greenland during the last interglaciation, The Cryosphere, 6, 1239–1250, https://doi.org/10.5194/tc-6-1239-2012, 2012.

Born, A., Imhof, M. A., and Stocker, T. F.: An efficient surface energy–mass balance model for snow and ice, The Cryosphere, 13, 1529–1546, https://doi.org/10.5194/tc-13-1529-2019, 2019.

Calov, R., Robinson, A., Perrette, M., and Ganopolski, A.: Simulating the Greenland ice sheet under present-day and palaeo constraints including a new discharge parameterization, The Cryosphere, 9, 179–196, https://doi.org/10.5194/tc-9-179-2015, 2015.

Capron, E., Govin, A., Feng, R., Otto-Bliesner, B. L., and Wolff, E. W.: Critical evaluation of climate syntheses to benchmark CMIP6/PMIP4 127 ka Last Interglacial simulations in the high-latitude regions, Quaternary Science Reviews, 168, 137–150, https://doi.org/10.1016/j.quascirev.2017.04.019, 2017.

Clark, P. U. and Huybers, P.: Interglacial and future sea level: Global change, Nature, 462, 856–857, http://doi.org/10.1038/462856a, 2009.

Colville, E. J., Carlson, A. E., Beard, B. L., Hatfield, R. G., Stoner, J. S., Reyes, A. V., and Ullman, D. J.: Sr-Nd-Pb isotope evidence for ice-sheet presence on southern Greenland during the Last Interglacial, Science, 333, 620–623, http://doi.org/10.1126/science.1204673, 2011.

Cuffey, K. M. and Marshall, S. J.: Substantial contribution to sea-level rise during the last interglacial from the Greenland ice sheet, Nature, 404, 591–594, https://doi.org/10.1038/35007053, 2000.

Cuffey, K. M. and Paterson, W.: The Physics of Glaciers, Elsevier Science, Burlington, 4th edn., 2010.

Cuzzone, J. K., Morlighem, M., Larour, E., Schlegel, N., and Seroussi, H.: Implementation of higher-order vertical finite elements in ISSM v4.13 for improved ice sheet flow modeling over paleoclimate timescales, Geosci. Model Dev., 11, 1683–1694, https://doi.org/10.5194/gmd-11-1683-2018, 2018.

de Ridder, K. and Gallée, H.: Land surface–induced regional climate change in southern Israel, Journal of Applied Meteorology, 37, 1470–1485, https://doi.org/10.1175/1520-0450(1998)037<1470:LSIRCC>2.0.CO;2, 1998.

Dutton, A., Carlson, A. E., Long, A. J., Milne, G. A., Clark, P. U., DeConto, R., Horton, B. P., Rahmstorf, S., and Raymo, M. E.: Sea-level rise due to polar ice-sheet mass loss during past warm periods, Science, 349, aaa4019, https://doi.org/10.1126/science.aaa4019, 2015.

Fettweis, X.: Reconstruction of the 1979–2006 Greenland ice sheet surface mass balance using the regional climate model MAR, The Cryosphere, 1, 21–40, https://doi.org/10.5194/tc-1-21-2007, 2007.

Fettweis, X., Gallée, H., Lefebre, F., and van Ypersele, J.-P.: The 1988–2003 Greenland ice sheet melt extent using passive microwave satellite data and a regional climate model, Climate Dynamics, 27, 531–541, https://doi.org/10.1007/s00382-006-0150-8, 2006.

Fettweis, X., Hanna, E., Gallée, H., Huybrechts, P., and Erpicum, M.: Estimation of the Greenland ice sheet surface mass balance for the 20th and 21st centuries, The Cryosphere, 2, 117–129, https://doi.org/10.5194/tc-2-117-2008, 2008.

5   Fettweis, X., Franco, B., Tedesco, M., Angelen, J. H. v., Lenaerts, J. T. M., Broeke, M. R. v. d., and Gallée, H.: Estimating the Greenland ice sheet surface mass balance contribution to future sea level rise using the regional atmospheric climate model MAR, The Cryosphere, 7, 469–489, https://doi.org/10.5194/tc-7-469-2013, 2013.

Fettweis, X., Box, J. E., Agosta, C., Amory, C., Kittel, C., Lang, C., van As, D., Machguth, H., and Gallée, H.: Reconstructions of the 1900–2015 Greenland ice sheet surface mass balance using the regional climate MAR model, The Cryosphere, 11, 1015–1033, https://doi.org/10.5194/tc-11-1015-2017, 2017.

10 Fyke, J. G., Weaver, A. J., Pollard, D., Eby, M., Carter, L., and Mackintosh, A.: A new coupled ice sheet/climate model: description and sensitivity to model physics under Eemian, Last Glacial Maximum, late Holocene and modern climate conditions, Geoscientific Model Development, 4, 117–136, https://doi.org/10.5194/gmd-4-117-2011, 2011.

Gallée, H. and Schayes, G.: Development of a three-dimensional meso-gamma primitive equation model: katabatic winds simulation in the area of Terra Nova Bay, Antarctica, Monthly Weather Review, 122, 671–685, https://doi.org10.1175/1520-0493(1994)122<0671: DOATDM>2.0.CO;2, 1994.

15 Gallée, H., Guyomarc'h, G., and Brun, E.: Impact of snow drift on the Antarctic ice sheet surface mass balance: possible sensitivity to snow-surface properties, Boundary-Layer Meteorology, 99, 1–19, https://doi.org/10.1023/A:1018776422809, 2001.

Goelzer, H., Huybrechts, P., Loutre, M.-F., and Fichefet, T.: Last Interglacial climate and sea-level evolution from a coupled ice sheet–climate model, Clim. Past, 12, 2195–2213, https://doi.org/10.5194/cp-12-2195-2016, 2016.

20 Greve, R.: Relation of measured basal temperatures and the spatial distribution of the geothermal heat flux for the Greenland ice sheet, Annals of Glaciology, 42, 424–432, https://doi.org/10.3189/172756405781812510, 2005.

Greve, R. and Blatter, H.: Dynamics of Ice Sheets and Glaciers, Springer, Berlin Heidelberg, https://doi.org/10.1007/978-3-642-03415-2, 2009.

25 Guo, C., Bentsen, M., Bethke, I., Ilicak, M., Tjiputra, J., Toniazzo, T., Schwinger, J., and Otterå, O. H.: Description and evaluation of NorESM1-F: a fast version of the Norwegian Earth System Model (NorESM), Geoscientific Model Development, 12, 343–362, https://doi.org/10.5194/gmd-12-343-2019, 2019.

Helsen, M. M., Wal, R. S. W. v. d., Broeke, M. R. v. d., Berg, W. J. v. d., and Oerlemans, J.: Coupling of climate models and ice sheet models by surface mass balance gradients: application to the Greenland Ice Sheet, The Cryosphere, 6, 255–272, https://doi.org/10.5194/tc-6-255-2012, 2012.

30 Helsen, M. M., Berg, W. J. v. d., Wal, R. S. W. v. d., Broeke, M. R. v. d., and Oerlemans, J.: Coupled regional climate–ice-sheet simulation shows limited Greenland ice loss during the Eemian, Clim. Past, 9, 1773–1788, https://doi.org/10.5194/cp-9-1773-2013, 2013.

Hutter, K.: Theoretical Glaciology: Material Science of Ice and the Mechanics of Glaciers and Ice Sheets, D. Reidel Publishing Company, Dordrecht, The Netherlands, 1983.

35 Huybrechts, P.: Sea-level changes at the LGM from ice-dynamic reconstructions of the Greenland and Antarctic ice sheets during glacial cycles, Quaternary Science Reviews, 21, 203–231, https://doi.org/10.1016/S0277-3791(01)00082-8, 2002.

Kopp, R. E., Simons, F. J., Mitrovica, J. X., Maloof, A. C., and Oppenheimer, M.: A probabilistic assessment of sea level variations within the last interglacial stage, Geophysical Journal International, p. ggt029, https://doi.org/10.1093/gji/ggt029, 2013.

Landais, A., Masson-Delmotte, V., Capron, E., Langebroek, P. M., Bakker, P., Stone, E. J., Merz, N., Raible, C. C., Fischer, H., Orsi, A., Prié, F., Vinther, B., and Dahl-Jensen, D.: How warm was Greenland during the last interglacial period?, Clim. Past, 12, 1933–1948, https://doi.org/10.5194/cp-12-1933-2016, 2016.

Larour, E., Seroussi, H., Morlighem, M., and Rignot, E.: Continental scale, high order, high spatial resolution, ice sheet modeling using the Ice Sheet System Model (ISSM), Journal of Geophysical Research: Earth Surface, 117, F01 022, https://doi.org/10.1029/2011JF002140, 2012.

Le clec'h, S., Charbit, S., Quiquet, A., Fettweis, X., Dumas, C., Kageyama, M., Wyard, C., and Ritz, C.: Assessment of the Greenland ice sheet–atmosphere feedbacks for the next century with a regional atmospheric model coupled to an ice sheet model, The Cryosphere, 13, 373–395, https://doi.org/10.5194/tc-13-373-2019, 2019.

Letréguilly, A., Reeh, N., and Huybrechts, P.: The Greenland ice sheet through the last glacial-interglacial cycle, Palaeogeogr., Palaeoclimatol., Palaeoecol. (Global Planet. Change Sect.), 90, 385–394, https://doi.org/10.1016/S0031-0182(12)80037-X, 1991.

Lhomme, N., Clarke, G. K. C., and Marshall, S. J.: Tracer transport in the Greenland Ice Sheet: constraints on ice cores and glacial history, Quaternary Science Reviews, 24, 173–194, https://doi.org/10.1016/j.quascirev.2004.08.020, 2005.

MacAyeal, D. R.: Large-scale ice flow over a viscous basal sediment: Theory and application to ice stream B, Antarctica, Journal of Geophysical Research: Solid Earth, 94, 4071–4087, https://doi.org/10.1029/JB094iB04p04071, 1989.

Morlighem, M., Rignot, E., Seroussi, H., Larour, E., Ben Dhia, H., and Aubry, D.: Spatial patterns of basal drag inferred using control methods from a full-Stokes and simpler models for Pine Island Glacier, West Antarctica, Geophysical Research Letters, 37, L14 502, https://doi.org/10.1029/2010GL043853, 2010.

Morlighem, M., Williams, C. N., Rignot, E., An, L., Arndt, J. E., Bamber, J. L., Catania, G., Chauché, N., Dowdeswell, J. A., Dorschel, B., Fenty, I., Hogan, K., Howat, I., Hubbard, A., Jakobsson, M., Jordan, T. M., Kjeldsen, K. K., Millan, R., Mayer, L., Mouginot, J., Noël, B. P. Y., O'Cofaigh, C., Palmer, S., Rysgaard, S., Seroussi, H., Siegert, M. J., Slabon, P., Straneo, F., van den Broeke, M. R., Weinrebe, W., Wood, M., and Zinglersen, K. B.: BedMachine v3: Complete bed topography and ocean bathymetry mapping of Greenland from multibeam echo sounding combined with mass conservation, Geophysical Research Letters, 44, 11,051–11,061, https://doi.org/10.1002/2017GL074954, 2017.

NEEM community members: Eemian interglacial reconstructed from a Greenland folded ice core, Nature, 493, 489–494, https://doi.org/10.1038/nature11789, 2013.

Otto-Bliesner, B. L., Marshall, S. J., Overpeck, J. T., Miller, G. H., and Hu, A.: Simulating Arctic climate warmth and icefield retreat in the last interglaciation, science, 311, 1751–1753, https://doi.org/10.1126/science.1120808, 2006.

Otto-Bliesner, B. L., Braconnot, P., Harrison, S. P., Lunt, D. J., Abe-Ouchi, A., Albani, S., Bartlein, P. J., Capron, E., Carlson, A. E., Dutton, A., Fischer, H., Goelzer, H., Govin, A., Haywood, A., Joos, F., LeGrande, A. N., Lipscomb, W. H., Lohmann, G., Mahowald, N., Nehrbass-Ahles, C., Pausata, F. S. R., Peterschmitt, J.-Y., Phipps, S. J., Renssen, H., and Zhang, Q.: The PMIP4 contribution to CMIP6 – Part 2: Two interglacials, scientific objective and experimental design for Holocene and Last Interglacial simulations, Geosci. Model Dev., 10, 3979–4003, https://doi.org/10.5194/gmd-10-3979-2017, 2017.

Overpeck, J., Otto-Bliesner, B. L., Miller, G., Muhs, D., Alley, R., and Kiehl, J.: Paleoclimatic evidence for future ice-sheet instability and rapid sea-level rise, Science, 311, 1747–1750, https://doi.org/10.1126/science.1115159, 2006.

Paterson, W.: The Physics of Glaciers (3rd edn), Pergamon Press, Oxford, 1994.

Pattyn, F.: A new three-dimensional higher-order thermomechanical ice sheet model: Basic sensitivity, ice stream development, and ice flow across subglacial lakes, Journal of Geophysical Research: Solid Earth, 108, https://doi.org/10.1029/2002JB002329, 2003.

Pfeffer, W. T., Harper, J. T., and O'Neel, S.: Kinematic constraints on glacier contributions to 21st-Century sea-level rise, Science, 321, 1340–1343, https://doi.org/10.1126/science.1159099, 2008.

Plach, A., Nisancioglu, K. H., Le clec'h, S., Born, A., Langebroek, P. M., Guo, C., Imhof, M., and Stocker, T. F.: Eemian Greenland SMB strongly sensitive to model choice, Climate of the Past, 14, 1463–1485, https://doi.org/10.5194/cp-14-1463-2018, 2018.

5 Price, S. F., Payne, A. J., Howat, I. M., and Smith, B. E.: Committed sea-level rise for the next century from Greenland ice sheet dynamics during the past decade, Proceedings of the National Academy of Sciences, 108, 8978–8983, https://doi.org/10.1073/pnas.1017313108, 2011.

Quiquet, A., Ritz, C., Punge, H. J., and Salas y Mélia, D.: Greenland ice sheet contribution to sea level rise during the last interglacial period: a modelling study driven and constrained by ice core data, Clim. Past, 9, 353–366, https://doi.org/10.5194/cp-9-353-2013, 2013.

10 Reeh, N.: Parameterization of melt rate and surface temperature on the Greenland ice sheet, Polarforschung, 59, 113–128, http://hdl.handle.net/10013/epic.13107, 1989.

Rignot, E. and Mouginot, J.: Ice flow in Greenland for the International Polar Year 2008–2009, Geophysical Research Letters, 39, L11 501, https://doi.org/10.1029/2012GL051634, 2012.

Ritz, C., Fabre, A., and Letréguilly, A.: Sensitivity of a Greenland ice sheet model to ice flow and ablation parameters: consequences for the 15 evolution through the last climatic cycle, Climate Dynamics, 13, 11–23, https://doi.org/10.1007/s003820050149, 1997.

Robel, A. A. and Tziperman, E.: The role of ice stream dynamics in deglaciation, Journal of Geophysical Research: Earth Surface, 121, 2016JF003 937, https://doi.org/10.1002/2016JF003937, 2016.

Robinson, A. and Goelzer, H.: The importance of insolation changes for paleo ice sheet modeling, The Cryosphere, 8, 1419–1428, https://doi.org/10.5194/tc-8-1419-2014, 2014.

20 Robinson, A., Calov, R., and Ganopolski, A.: Greenland ice sheet model parameters constrained using simulations of the Eemian Interglacial, Clim. Past, 7, 381–396, https://doi.org/10.5194/cp-7-381-2011, 2011.

Schlegel, N.-J., Larour, E., Seroussi, H., Morlighem, M., and Box, J. E.: Decadal-scale sensitivity of Northeast Greenland ice flow to errors in surface mass balance using ISSM, Journal of Geophysical Research: Earth Surface, 118, 667–680, https://doi.org/10.1002/jgrf.20062, 2013.

25 Shapiro, N. and Ritzwoller, M.: Inferring surface heat flux distributions guided by a global seismic model: particular application to Antarctica, Earth and Planetary Science Letters, 223, 213–224, https://doi.org/10.1016/j.epsl.2004.04.011, 2004.

Stone, E. J., Lunt, D. J., Annan, J. D., and Hargreaves, J. C.: Quantification of the Greenland ice sheet contribution to Last Interglacial sea level rise, Clim. Past, 9, 621–639, https://doi.org/10.5194/cp-9-621-2013, 2013.

Straneo, F. and Heimbach, P.: North Atlantic warming and the retreat of Greenland's outlet glaciers, Nature, 504, 36–43, 30 doi:10.1038/nature12854, http://www.nature.com/nature/journal/v504/n7478/abs/nature12854.html, 2013.

Tabone, I., Blasco, J., Robinson, A., Alvarez-Solas, J., and Montoya, M.: The sensitivity of the Greenland Ice Sheet to glacial–interglacial oceanic forcing, Clim. Past, 14, 455–472, https://doi.org/10.5194/cp-14-455-2018, 2018.

Tarasov, L. and Richard Peltier, W.: Greenland glacial history and local geodynamic consequences, Geophysical Journal International, 150, 198–229, https://doi.org/10.1046/j.1365-246X.2002.01702.x, 2002.

35 van de Berg, W. J., van den Broeke, M., Ettema, J., van Meijgaard, E., and Kaspar, F.: Significant contribution of insolation to Eemian melting of the Greenland ice sheet, Nature Geoscience, 4, 679–683, https://doi.org/10.1038/ngeo1245, 2011.

Yin, Q. and Berger, A.: Interglacial analogues of the Holocene and its natural near future, Quaternary Science Reviews, 120, 28–46, https://doi.org/10.1016/j.quascirev.2015.04.008, 2015.

Zwally, H. J., Abdalati, W., Herring, T., Larson, K., Saba, J., and Steffen, K.: Surface melt-induced acceleration of Greenland ice-sheet flow, Science, 297, 218–222, https://doi.org/10.1126/science.1072708, 2002.